Suspended Manufacture of Biological Structures

Moxon, Samuel R.; Cooke, Megan E; Cox, Sophie; Snow, Martyn; Jeys, L; Jones, Simon; Smith, Alan M.; Grover, Liam

DOI:
10.1002/adma.201605594

Document Version
Publisher's PDF, also known as Version of record

Citation for published version (Harvard):
Moxon, SR, Cooke, ME, Cox, S, Snow, M, Jeys, L, Jones, S, Smith, AM & Grover, L 2017, 'Suspended Manufacture of Biological Structures', Advanced Materials, vol. 29, no. 13, 1605594. https://doi.org/10.1002/adma.201605594

COMMUNICATION

Suspended Manufacture of Biological Structures

Samuel R. Moxon, Megan E. Cooke, Sophie C. Cox, Martyn Snow, Lee Jeys, Simon W. Jones, Alan M. Smith, and Liam M. Grover**

In this study, we describe a novel method of suspended manufacture for the production of complex soft structures of closely defined morphology, mechanical properties, and chemistry. The process conditions are sufficiently mild that embedded populations of cells maintain high levels of viability and retain phenotype. Given the simplicity of the process, it can be used for all existing gel materials without special modification. The method of manufacturing uses a "bed" of micrometer sized gel particles (often referred to as fluid or sheared gels),[1] which behave in bulk as a viscoelastic fluid and can self-heal thereby providing support to the complete part.[2] The final structure is formed through the dispersion of a gelling material into the interstices between the supporting fluid gel particles. This enables relatively complex structuring while providing sufficient support to prevent the structure collapsing under its own weight. Once the scaffold structure has been formed the supporting phase may be removed through the gentle application of shear. This manufacturing process allows for the use of a wide range of polymeric materials, including many already approved by regulatory bodies. Ultimately it has the potential to produce structures that could make their way into clinical trial in the relative short term. Here we demonstrate the power of this method by manufacturing anisotropic structures with spatially controlled mechanical and chemical properties, which support a coculture of viable cells. These scaffolds could be used for the production of osteochondral plugs for the augmentation of full-thickness cartilage defects.

Tissues are formed of populations of cells distributed within an extracellular matrix (ECM), which is structured down to the molecular level. Local variations in organization and biochemistry mean that the encapsulated populations of cells are exposed to environments that differ both mechanically and chemically. These environments have been shown to play a strong role in shaping cell phenotype.[3] For some time now researchers have sought to recapitulate tissue structure using a combination of isolated cells and polymeric hydrogels that have a structural resemblance to the ECM.[4] Such specimens have been manufactured using the process of gel-casting; this allows for gross geometrical control, yet provides little control over the microscale geometry and spatial and mechanical cues important to controlling cell behavior.[5] Additive layer manufacturing (ALM) offers the tantalizing possibility of creating structures with a greater level of complexity than traditional processing methods such as casting, and some degree of control over the distribution of cells and other important components throughout the structure. While the ALM of hard materials is relatively mature and a number of industries now utilize such technologies, at present the ALM of soft materials remains challenging. ALM using soft materials has been reported in the literature since the mid 2000s when Boland et al. published on the production of "nose-like" specimens from alginate.[6] In the years since many research groups have published on the manufacture of structures from soft solids some of which allow for the incorporation of cells.[7] Most recently, Hwang et al. reported the production of a cartilage-like structure for auricular reconstruction.[8] Notably, the majority of additively manufactured soft-solid structures exhibit relatively low complexity[9] and are typically broader at their base than at their peak to reduce the risk of the structure collapsing. A number of research groups are working on the development of novel polymers for ALM,[7,10] but in the most part, the structures they form with these polymers are highly simplistic, with a self-supporting "waffle arrangement" frequently being used to demonstrate process resolution.[7,9,11] Some papers report the use of harder materials, such as poly(caprolactone) (PCL) and hydroxyapatite, to support the structure[12,13] or have extruded materials into high viscosity liquids, for example Pluronic F-127 hydrogel.[13] Additionally, there have been reports of additive manufacturing using a suspending medium that consists of either a shear-thinning synthetic hydrogel[14] or a slurry of gelatin particles,[15] respectively. These elegant approaches resulted in structures of previously unprecedented complexity, but neither group managed to codeposit multiple cell types or could demonstrate any localized modification in mechanical properties of chemistry, both of which are critical to biological performance. Furthermore, neither of these methods is conducive to the manufacture of structures that are suitable for the clinic, since the suspending medium would be very challenging to completely remove from the finished part. In this study, we have addressed these issues by using a self-healing particulate or fluid gel material, which is stable at room temperature and in culture conditions, as a

S. R. Moxon, Dr. A. M. Smith
Department of Pharmacy
University of Huddersfield
Queensgate, Huddersfield HD1 3DH, UK
E-mail: a.m.smith@hud.ac.uk
M. E. Cooke, Dr. S. C. Cox, Prof. M. Snow, Prof. L. M. Grover
School of Chemical Engineering
University of Birmingham
Edgbaston B15 2TT, UK
E-mail: l.m.grover@bham.ac.uk
M. E. Cooke, Dr. S. W. Jones
Institute of Inflammation and Ageing
MRC Musculoskeletal Ageing Centre
QE Hospital
University of Birmingham
Edgbaston B15 2WB, UK
Prof. M. Snow, Prof. L. Jeys
Royal Orthopaedic Hospital
Bristol Road, Northfield, Birmingham B31 2AP, UK

DOI: 10.1002/adma.201605594

supporting media. The strong surface interactions between gel particles form short-range adhesions when in close contact causing the paste-like material to thicken.[16] The interactions formed between the particles allow the particulate material to support a secondary phase of similar (or in some cases higher) density. This "true-gel" ($G' >>> G''$) particulate (Figures S1–S3, Supporting Information) microstructure makes this system physically distinct from highly viscous fluids, such as commercial shower gels, that are formed almost exclusively by polymer entanglement.[17] Importantly, since the gel particles are discrete entities they do not contaminate the surface of the manufactured sample and can actually be formed from the same material as that extruded into the particle bed (**Figure 1**) likely simplifying the translational pathway. Using particulate gels as a suspending agent, supports the fragile construct as it is formed, in a similar manner to the way amniotic fluid suspends the developing fetus. Using an XYZ stage, it was possible to (with 100 µm resolution) deposit the hydrogel polymer in a discrete 3D location, the resolution of which is limited only by the size of the droplet from the end of the extruding needle and the viscosity of the supporting medium.

A variety of hydrogel materials may be used for the production of the final part and the supporting bed. Initial experimentation demonstrated that it was possible to generate structures using combinations of gelatin, gellan, collagen, hyaluronic acid, agarose, and alginate. As a consequence of its relative robustness and capacity for physical modification using seeded hydroxyapatite,[18] gellan was selected for further use as the final part and agarose as the supporting bed. The supporting bed, formed from agarose with particles in the size range 2–11 µm (Figure S4, Supporting Information), was of sufficient robustness to suspend a cross-linked gellan gum structure such as the helix illustrated in Figure 1. This helical structure was loaded with colloidal hydroxyapatite nanocrystals in order to increase radio-opacity enabling micro-computed tomography (CT) imaging. Following treatment with calcium chloride solution this helical structure was removed from the particle bed and was shown to be self-supporting (Figure 1). The shear forces applied during the extrusion process were not of sufficient magnitude to cause phase separation and were sufficiently mild that it was possible to maintain the viability of a population of human primary chondrocytes within the cultures (**Figure 2**). To investigate the influence of supporting matrix viscosity on the resolution of the printing method, samples were made using a controlled concentration of gellan gum (1.5%) and a hypodermic needle of internal diameter 337 µm. An increase in the viscosity of the supporting medium resulted in a monotonic increase in resolution in the *XY* dimensions, but interestingly a smaller reduction in resolution in the *Z* dimension (Figure 2). At this scale, resolution is ultimately limited by droplet size, which is controlled by the internal dimensions, flow rate of the extruding aperture and other parameters of deposition, such as the viscosity of the extruded solutions. To further investigate factors that may influence resolution, structures were formed using a range of needle diameters and it was demonstrated that resolution was

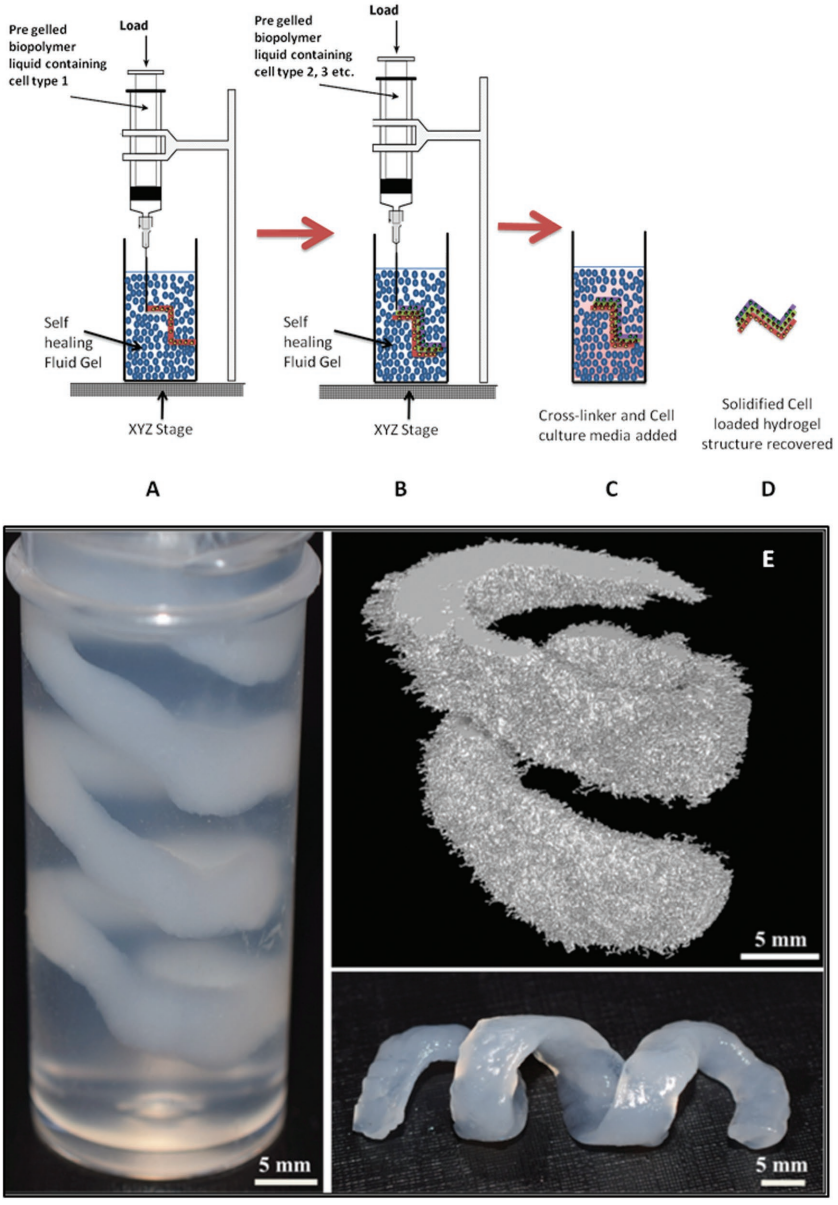

Figure 1. A–D) A schematic showing the manufacturing process for a 3D soft solid structure manufactured using the suspended deposition method. A) Briefly, a supporting "fluid-gel" matrix is created in a vessel. B) A secondary phase may then be extruded into the particle bed. C) The self-healing, fluid gel supports the gel structure during the cross-linking process. D) Once cross-linked, the object may be removed from the particle bed. E) This was manipulated to fabricate a simple helix loaded with hydroxyapatite nanoparticles and imaged with micro-CT (scale bars = 5 mm).

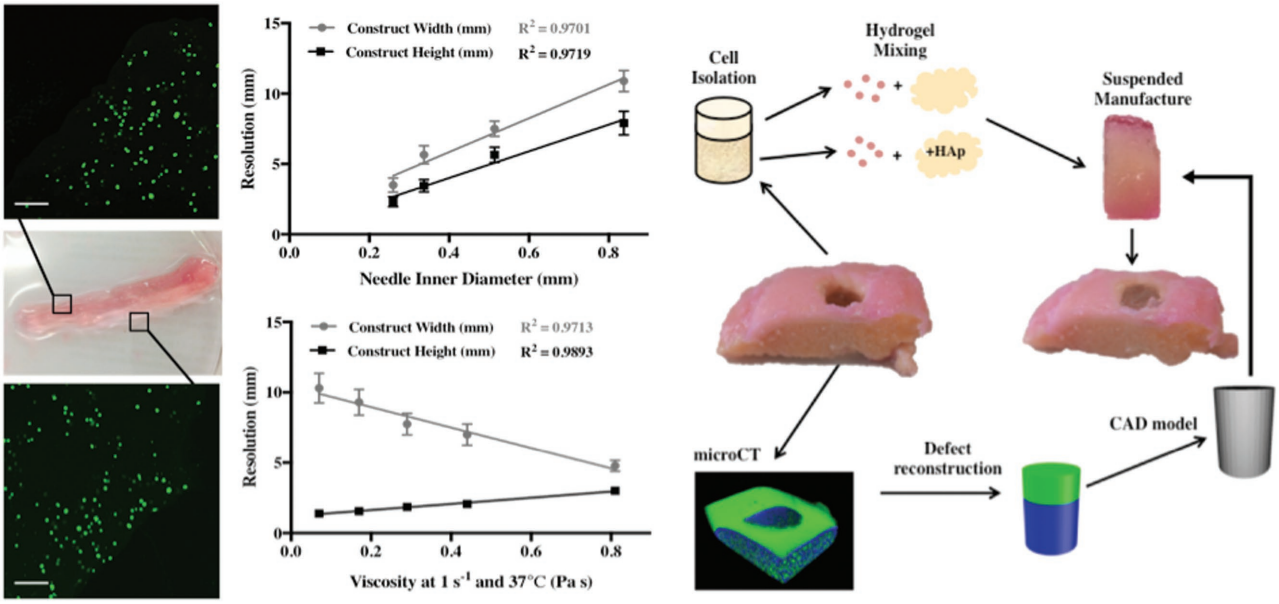

Figure 2. Extrusion of a gellan matrix loaded with primary human chondrocytes into the "fluid-gel" structure through a 337 µm internal diameter needle maintained cell viability throughout the construct (left column, scale bars = 200 µm). An increase in the internal diameter of the needle resulted in a reduction in resolution (centre, top), as did a reduction in the viscosity of the matrix (centre, bottom). From these experiments, a fluid viscosity of 0.75 Pa s (at 1 s^{-1} shear rate) and needle diameter of 337 µm was set for manufacture of an osteochondral plug. A computer model of this plug (right column) was generated from CT scans of a defect drilled into the tissue by a clinician. The model generated was used to inform the manufacture of a plug with appropriate chondral and subchondral thicknesses to fit the tissue defect.

directly related to needle diameter, increasing up to the point that the hydrocolloid could no longer be extruded (Figure 2). The peak resolution achievable for the 1.5% gellan gum and the agarose supporting medium was 250 µm. Given the scale of the tissues to be produced for osteochondral repair and the need for cell viability, the needle diameter was set at 337 µm and extrusion rate no more than 125 µL s^{-1}. To demonstrate the complexity achievable with the suspended manufacturing process, scaffolds that mimic the structuring and cellular organization of an osteochondral defect were manufactured. This complex tissue region lies between articular cartilage and bone on an articulating joint surface[19] and may be severely damaged following trauma[20] or can deteriorate during the progression of osteoarthritis.[21] At present the standard of care is microfracture in the knee[22] or the transplantation of tissue that has been isolated from a cadaver or nonarticulating region of the joint.[22] Neither method has been shown to be absolutely successful and this has driven research into the development of a range of synthetic osteochondral plugs.[23] The main reason for failure of these synthetic grafts is through delamination at the hard–soft tissue interface.[24] Native osteochondral tissue exhibits a gradual structural change from disordered mineralized collagen at the subchondral bone,[25] through to collagen II and glycosaminoglycan (GAG) - rich cartilage[26] allowing stress to be distributed across the interface without stress localization and delamination occurring.[26,27] The region consists of four principle cells types, which secrete and organize their local environments.[25,26] Although a number of groups have attempted this in vitro[28] the processes that they have employed did not mimic the structuring of this complex structure at a length-scale that is appropriate to the size of the defects encountered clinically.

Here, the suspended manufacturing process was used to form composite hydrogel structures with anisotropic mechanical properties mimicking the native osteochondral environment. Femoral condyle tissue was retrieved from patients following knee replacement and an osteochondral defect was introduced using a surgical drill. Excess retrieved tissues were digested to release the cells from the cartilage and bone samples. The structure was scanned using micro-CT and a 3D model of the defect was created. This 3D model was used to guide the manufacture of an osteochondral implant where the lower surface was loaded with sol-HA, gellan, and osteoblast cells (**Figure 3**). The upper surface of the construct was manufactured using gellan gum alone, loaded with populations of chondrocytes (Figure 3). The suspended manufacturing process allowed for the production of osteochondral structures that fit tightly into the defects and matched the layer thicknesses for the bone and cartilage components. These samples were then placed in culture for a period of four weeks in order to identify whether the cell types in the different regions of the defect maintained phenotype. Over the course of four weeks of in vitro culture the osteochondral plugs maintained their structural integrity; they could be easily handled and extracted from the defect without deterioration (Figure 3).

Mechanical spectra of the osteochondral constructs highlight the successful integration of two different materials into a single structure (Figure 3). Constructs were sliced into four regions and stress sweeps were conducted on each section to determine mechanical strength and elasticity. Samples were subjected to increasing stress (0.1–1000 Pa) and a range of mechanical properties was observed throughout the construct. The weakest areas with the shortest linear viscoelastic

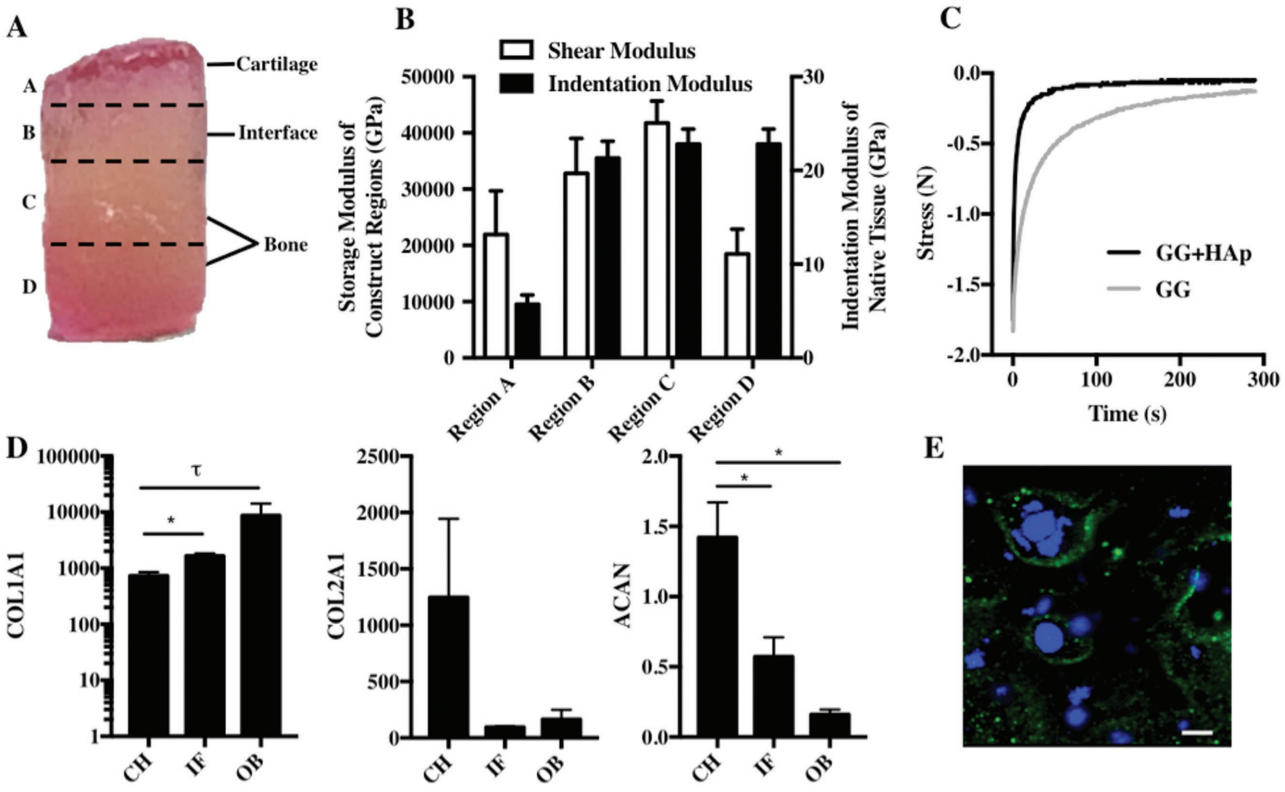

Figure 3. A) Samples manufactured using suspended manufacturing were cultured before being cut with a razor blade and mechanically characterized using a rheometer. B) The storage modulus of the construct reduced significantly from the core "boney" area of the structure (Regions C and D) into the chondral region (Regions A and B). Mechanical data reflected trends seen in native tissue with an increase in modulus from hyaline cartilage (Region A) through the osteochondral interface (Region B) to subchondral bone (Regions C and D).[20] This demonstrates that it is possible to not only define geometric but also the mechanical properties exhibited by the resulting structure. C) Stress relaxation measurements show that the addition of hydroxyapatite (GG + HAp) results in a faster relaxation response than gellan gum alone (GG). D) Following 4 weeks of culture within the human tissue defects ($n = 6$), the construct was removed and cells within the cartilage (CH), interfacial (IF) and bone (OB) regions were recovered for RNA isolation and mRNA was analyzed by qRT-PCR. The cells in the cartilaginous section of the scaffold expressed the highest levels of coll II and aggrecan (ACAN) and the bone region expressed significantly more coll IA1 (mean ± SEM). This suggests that the cells deposited into discrete regions maintained not only viability but also their phenotype (*: $P < 0.05$, τ: $P = 0.0793$). E) Fluorescent immunohistochemistry (IHC) (DAPI (4,6-Ddamidino-2-phenylindole) = blue, aggrecan = green) shows the production of aggrecan in the cartilaginous region of the structure (scale bars = 200 µm).

region were the chondral region and the uppermost surface of the construct (Regions A and D). Region C exhibited significantly higher gel strength and elasticity. This can be attributed to the nanocrystalline hydroxyapatite (nano-HA) interacting with gellan helices during gelation to create a highly homogenous structure exhibiting higher strength in comparison with unloaded gellan (Figure 3). Interestingly, the incorporation of HA into the gellan hydrogel resulted in a more rapid relaxation response than the gellan alone (Figure 3C). This is significant since matrices of elastic modulus >17 kPa that exhibit more rapid stress relaxation encourage mineralization to a greater extent when compared with those with slower stress response.[29] Region A was comprised entirely of gellan gum without nano-HA, which explains the lower gel strength. It is likely that the nano-HA began to sediment prior to gelation due to its higher density compared with the gel phase (3.16 compared with ≈1 g cm^{-3}) resulting in the top of the osteogenic region showing a lower modulus. At the interface (Region B), the construct exhibited mechanical properties intermediate to Regions A and C providing evidence for a successful integration of the two different materials (Figure 3). Interestingly, the trend in mechanical properties observed in regions A–C shows some similarity to reported changes in modulus across osteochondral tissue (Figure 3). A 2012 study by Campbell et al. outlined indentation moduli of three osteochondral regions, namely subchondral bone, hyaline cartilage, and the osteochondral interface.[27] Subchondral bone exhibited the highest modulus, hyaline cartilage the lowest with calcified cartilage (the interface) falling between the two, albeit closer to the modulus of bone. Indentation moduli of tissue regions were orders of magnitudes greater than storage moduli of respective construct regions and methods used to determine both differed greatly. However, parallels between the two trends highlight the level of control exhibited over mechanical properties within each region of osteochondral constructs.

Polymerase chain reaction (PCR) data collected from the retrieved samples demonstrated that the expression of both collagen type II and aggrecan (ACAN) (both markers of cartilage formation) was highest in the chondral region of the scaffold (Figure 3) and collagen type I expression was lowest at this point. Immunohistochemical (IHC) analysis of the samples demonstrated the presence of aggrecan around the encapsulated

cells in this area of the scaffold (Figure 3). Remarkably, the ratio of collagen II to collagen I changed gradually throughout the structure inline with what would be expected with the native tissue region. This indicated that while the two sections of the osteochondral scaffold were well integrated, the embedded cell population retained their native phenotype. This is something that has proven challenging with existing technologies for tissue structuring. In comparison with the majority of ALM methods, where high temperatures, pressures, or cross-linking agents are a necessity, the suspended manufacture method allowed us to maintain viability and behavior while subtly modifying the local composition of the matrix.

In this paper, a new method was reported to manufacture comparatively complex soft-solid structures by extruding a gelling polymer into a supporting particle-based matrix. The method allowed the structuring of soft-solid materials such that they exhibited distinct chemical and physical properties on the microscale. It was shown that suspended manufacture could recapitulate the structure of the osteochondral region as defined by CT scanning. The printed structure maintained its morphology and mechanical robustness over a period of four weeks of culture during which the encapsulated cells retained their phenotype. Our findings suggest that this novel method of producing 3D tissue-like structures has significant promise for the regeneration and study of complex tissue structures and interfaces.

Experimental Section

Fluid Gel Formulation: Fluid gels were manufactured by cooling solutions of 0.5% w/w agarose from 85 to 20 °C under constant shear using a magnetic stirrer rotating at 700 rpm. This created a constant angular velocity of 74 rad s^{-1}. Fluid gels were sterilized for cell culture applications by autoclaving agarose solutions prior to cooling.

Suspension of Helical Polymeric Structures: Aliquots of fluid gel were prepared in 6 mL Bijoux tubes. Solutions of 1.5% w/w low acyl gellan mixed with 10% nanocrystalline hydroxyapatite/HA at 60 °C (formulated by a precipitation method)[30] were extruded into fluid gel samples through a hypodermic needle with a 337 µm inner diameter using a 5 mL syringe. During extrusion, the syringe was manipulated precisely with respect to geometric position to enable the generation of the helix. The suspensions were then left at room temperature for 40 min to enable gelation to occur. Prior to extraction, samples were observed using micro-CT (Bruker Skyscan 1172—Bruker, Belgium) and reconstructed data were visualized in 3D using CTVox software (Bruker). Helices were then extracted and excess fluid gel was washed away with deionized water.

Tuning Resolution of Suspended Constructs: Low acyl gellan gum solutions of varying viscosity (as controlled by polymer concentration) were extruded into separate aliquots of fluid gel (contained in petri dishes of 60 mm diameter and 15 mm depth). Gelation was triggered by temperature and ionic interaction via injection of 200×10^{-3} M $CaCl_2$ around constructs at 20 °C. After 30 min, gelled structures were extracted and the resolution of each construct was measured.

Evaluation of Cell Culture Applications: Osteochondral tissue was donated by patients undergoing elective knee replacement surgery. This study was approved by the United Kingdom National Ethics Research Committee (Hertfordshire Research Ethics Committee 12/EE/0136). Articular cartilage was removed from human femoral condyle tissue before mincing and digestion by 2 mg mL^{-1} collagenase for 4 h under agitation at 37 °C for release of chondrocytes. Bone chips (4–5 mm^3) from subchondral trabecular bone were cultured for release of osteoblasts. Both cell types were cultured in Dulbecco's modified Eagle's medium (DMEM) supplemented with 10% fetal bovine serum, 1% L-glutamine, 1% PenStrep, and 1% nonessential amino acids. At passage 1, cells were trypsinized, counted, and resuspended at a density of 3×10^6 cells mL^{-1} before being mixed with sterile 1.5% low acyl gellan gum. Cell-laden gellan gum was extruded into sterile agarose fluid gel to create linear constructs. Gelation at 20 °C was triggered with 200×10^{-3} M $CaCl_2$ and excess calcium ions were washed away after 30 min using Dulbecco's phosphate buffered saline (PBS). Cell-loaded constructs were cultured at 37 °C/5% CO_2 in culture media (as above). Cell viability was visualized using Calcein-acetoxymethyl (AM) and ethidium homodimer-1 fluorescent dyes.

Defect Formation and Reconstruction: Defects were introduced into femoral condyle tissue following surgery using an orthopedic drill. The resulting tissue was imaged using microCT (Bruker Skyscan 1172) and reconstructed data were viewed using CTVox software (Bruker). The defect was then measured for reconstruction of the defect space in Simpleware (Synopsys, UK).

Implant Fabrication and Culture: Prior to implant fabrication cells were isolated and cultured as above. Primary human osteoblasts and chondrocytes were trypsinized, counted, and resuspended at a density of 1×10^6 cells mL^{-1}. Osteoblasts were loaded into 1.5% low acyl gellan mixed with 5% nano-HA while chondrocytes were mixed with 1.5% gellan. Guided by dimensions obtained from defect reconstruction, single implants were fabricated containing a layer of chondrocyte-loaded gellan and a thicker layer of osteoblast-loaded gellan/HA via extrusion into sterile agarose fluid gel. Gelation at 20 °C was triggered with injection of 200×10^{-3} M $CaCl_2$ around each suspended structure and constructs were extracted after 30 min. Excess fluid gel was washed away and constructs were implanted into tissue defects. The construct-filled defects were then cultured as above in a humidified incubator at 37 °C, 5% CO_2 for 30 d ($n = 6$).

Determination of Collagen 1, Collagen 2, and Aggrecan (ACAN) Expression: Following 30 d of culture, constructs were removed from the tissue defects and separated into cartilage, interface, and bone regions for gene expression analysis. RNA was isolated using TRIZol reagent (Life Technologies, UK) and the manufacturer's instructions were followed. RNA was quantified using photospectrometry (NanoDrop 2000, NanoDrop Technologies). Quantitative-realtime polymerase chain reaction (Q-RTPCR) was performed using a Lightcycler 480 (Roche). The expression of collagen type I, type II, and aggrecan (ACAN) were measured and normalized to 18S expression. Validated TaqMan probes were purchased from Life Technologies. Gene expression was quantified using the Pfaffl method.[31]

Fluorescent Immunohistochemistry: Constructs were fixed with 4% paraformaldehyde before blocking in vehicle (10% goat serum, 0.1 M PBS, 0.3% Triton-X-100). For aggrecan, cells were incubated with mouse antiaggrecan primary antibody (1:100, ThermoFisher) and then Alexa 488 goat antimouse secondary antibody (1:500, Invitrogen). Nuclei were stained with 4,6-Diamddino-2-phenylindole (DAPI) (1:5000, Sigma-Aldrich) and constructs were imaged using a Leica DM 6000B microscope.

Mechanical Spectra of Implants: Layered constructs were sliced laterally into four separate regions (see Figure 3—mechanical spectra figure). Stress sweeps were conducted on each region using a Bohlin Gemini rheometer (Malvern, UK) with 25 mm serrated parallel plate geometry. Elastic and viscous moduli (G' and G'', respectively) were analyzed in response to increasing stress from 1 to 100 Pa at a constant temperature of 37 °C. For stress relaxation, gellan gum and gellan gum/hydroxyapatite constructs (height 8 mm, diameter 14 mm) were displaced 2 mm and held for 300 s while load was recorded (Bose ElectroForce 5500).

Rheological Measurements: All rheological measurements were performed on a Bohlin Gemini rheometer (Malvern, UK) using a 55 mm 2° cone and plate geometry at an isothermal temperature of 37 °C which was maintained by a Peltier controlled lower plate.

Stress Sweeps: Samples of 0.5% agarose fluid gels were prepared and loaded onto the bottom plate of the rheometer. The samples were then

subjected to a shear stress range of 0.1–100 Pa at a constant oscillatory frequency of 10 Rad s^{-1}. Elastic and viscous moduli were measured in response to increasing shear stress. Results were analyzed to determine the linear viscoelastic region.

Frequency Sweeps: Elastic and viscous moduli of 0.5% agarose fluid gels were analyzed in response to increasing oscillatory frequencies from 0.1 to 10 Rad s^{-1} at a constant strain of 0.05%.

Shear Sweeps: Shear ramps were performed at 37 °C on 0.5% agarose fluid gel samples. Shear rate was increased from 0.001 to 100 s^{-1} over a 10 min period and dynamic viscosity in response to increasing shear rate was subsequently analyzed.

Particle Size Distribution: Fluid gel samples were loaded onto glass slides and allowed to dry under a coverslip for 10 min. Samples were then visualized on Keyence VHX 2000 digital microscope (Keyence, UK). Particle sizes were analyzed with VHX 2000 communication software. Particle size distribution was evaluated using images of fluid gel particles within an area of 135 μm × 120 μm. Images were divided into 12 grids of 11.25 μm × 10 μm. Within each grid, the number of particles was recorded and divided into categories based on size. A total of 96 grids and ≈2300 particles were counted. Particle size distribution was subsequently determined by comparing the number of particles within each size range and calculating cumulative undersize.

Supporting Information

Supporting Information is available from the Wiley Online Library or from the author.

Acknowledgements

S.R.M. and M.E.C. contributed equally to this work. The authors would like to acknowledge the EPSRC for the provision of a studentship (M.E.C.) through the Sci-Phy-4-Health Centre for Doctoral Training (EP/L016346/1) and the University of Huddersfield for funding the Studentship of S.R.M.

Received: October 17, 2016
Revised: December 11, 2016
Published online: February 1, 2017

[1] a) I. T. Norton, D. A. Jarvis, T. J. Foster, *Int. J. Biol. Macromol.* **1999**, *26*, 255; b) I. Fernandez Farres, R. J. A. Moakes, I. T. Norton, *Food Hydrocolloids* **2014**, *42*, 362.
[2] A. Gabriele, F. Sypyropoulos, I. T. Norton, *Food Hydrocolloids* **2009**, *23*, 2054.
[3] J. Y. Rho, L. Kuhn-Spearing, P. Zioupos, *Med. Eng. Phys.* **1998**, *20*, 92.
[4] M. W. Tibbitt, K. S. Anseth, *Biotechnol. Bioeng.* **2009**, *103*, 655.
[5] J. L. Vanderhooft, M. Alcoutlabi, J. J. Magda, G. D. Prestwich, *Macromol. Biosci.* **2009**, *9*, 20.
[6] T. Boland, X. Tao, B. J. Damon, B. Manley, P. Kesari, S. Jalota, S. Bhaduri, *Mater. Sci. Eng. C* **2006**, *27*, 372.
[7] S. Hong, D. Sycks, H. F. Chan, S. Lin, G. P. Lopez, F. Guilak, K. W. Leong, X. Zhao, *Adv. Mater.* **2015**, *27*, 4035.
[8] C. M. Hwang, B. K. Lee, D. Green, S. Y. Jeong, G. Khang, J. D. Jackson, A. Atala, S. J. Lee, J. J. Yoo, *Plast. Reconstr. Surg.* **2014**, *133*, 360e.
[9] M. Costantini, J. Idaszek, K. Szoke, J. Jaroszewicz, M. Dentini, A. Barbetta, J. E. Brinchmann, W. Swieszkowski, *Biofabrication* **2016**, *8*, 035002.
[10] a) T. Jungst, W. Smolan, K. Schacht, T. Scheibel, J. Groll, *Chem. Rev.* **2016**, *116*, 1496; b) D. Chimene, K. K. Lennox, R. R. Kaunas, A. K. Gaharwar, *Ann. Biomed. Eng.* **2016**, *44*, 2090.
[11] D. A. Zopf, A. G. Mitsak, C. L. Flanagan, M. Wheeler, G. E. Green, S. J. Hollister, *Otolaryngol.–Head Neck Surg.* **2015**, *152*, 57.
[12] a) F. P. Melchels, M. M. Blokzijl, R. Levato, Q. C. Peiffer, M. Ruijter, W. E. Hennink, T. Vermonden, J. Malda, *Biofabrication* **2016**, *8*, 035004; b) E. Sachlos, D. Gotora, J. T. Czernuszka, *Tissue Eng.* **2006**, *12*, 2479.
[13] H. W. Kang, S. J. Lee, I. K. Ko, C. Kengla, J. J. Yoo, A. Atala, *Nat. Biotechnol.* **2016**, *34*, 312.
[14] C. B. Highley, C. B. Rodell, J. A. Burdick, *Adv. Mater.* **2015**, *27*, 5075.
[15] T. J. Hinton, Q. Jallerat, R. N. Palchesko, J. H. Park, M. S. Grodzicki, H.-J. Shue, M. H. Ramadan, A. R. Hudson, A. W. Feinberg, *Sci. Adv.* **2015**, *9*, e1500758.
[16] I. T. Norton, D. A. Jarvis, T. J. Foster, *Int. J. Biol. Macromol.* **1999**, *26*, 255.
[17] a) R. J. Crawford, K. J. Edler, S. Lindhoud, J. L. Scott, G. Unali, *Green Chem.* **2012**, *14*, 300; b) I. Avramov, *J. Non-Cryst. Solids* **2005**, *351*, 3163.
[18] a) P. Jamshidi, P. Ma, K. Khosrowyar, A. M. Smith, L. M. Grover, *J. Exp. Nanosci.* **2012**, *7*, 652; b) P. Jamshidi, G. Birdi, R. L. Williams, S. C. Cox, L. M. Grover, *Biotechnol. Bioeng.* **2015**, *113*, 1568.
[19] M. Keeney, A. Pandit, *Tissue Eng., Part B* **2009**, *15*, 55.
[20] K. D. Shelbourne, S. Jari, T. Gray, *J. Bone Joint Surg. Am.* **2003**, *85-A*, 8.
[21] M. B. Goldring, *HSS J.* **2012**, *8*, 7.
[22] R. Gudas, R. J. Kalesinskas, V. Kimtys, E. Stankevicius, V. Toliusis, G. Bernotavicius, A. Smailys, *Arthroscopy* **2005**, *21*, 1066.
[23] a) J. K. Sherwood, S. L. Riley, R. Palazzolo, S. C. Brown, D. C. Monkhouse, M. Coates, L. G. Griffith, L. K. Landeen, A. Ratcliffe, *Biomaterials* **2002**, *23*, 4739; b) I. Martin, S. Miot, A. Barbero, M. Jakob, D. Wendt, *J. Biomech.* **2007**, *40*, 750.
[24] a) C. A. Robb, C. El-Sayed, G. S. Matharu, K. Baloch, P. Pynsent, *Acta Orthop. Belg.* **2012**, *78*, 643; b) T. L. Nosewicz, M. L. Reilingh, C. N. van Dijk, G. N. Duda, H. Schell, *Knee Surg. Sports Traumatol. Arthrosc.* **2012**, *20*, 1919.
[25] M. B. Goldring, S. R. Goldring, *Ann. N. Y. Acad. Sci.* **2010**, *1192*, 230.
[26] A. J. S. Fox, A. Bedi, S. A. Rodeo, *Sports Health* **2009**, *1*, 461.
[27] a) S. E. Campbell, V. L. Ferguson, D. C. Hurley, *Acta Biomater.* **2012**, *8*, 4389; b) V. L. Ferguson, A. J. Bushby, A. Boyde, *J. Anat.* **2003**, *203*, 191.
[28] a) D. Puppi, C. Mota, M. Gazzarri, D. Dinucci, A. Gloria, M. Myrzabekova, L. Ambrosio, F. Chiellini, *Biomed. Microdev.* **2012**, *14*, 1115; b) H.-W. Cheng, K. D. K. Luk, K. M. C. Cheung, B. P. Chan, *Biomaterials* **2011**, *32*, 1526; c) J. M. Oliveira, M. T. Rodrigues, S. S. Silva, P. B. Malafaya, M. E. Gomes, C. A. Viegas, I. R. Dias, J. T. Azevedo, J. F. Mano, R. L. Reis, *Biomaterials* **2006**, *27*, 6123.
[29] O. Chaudhuri, L. Gu, D. Klumpers, M. Darnell, S. A. Bencherif, J. C. Weaver, N. Huebsch, H. P. Lee, E. Lippens, G. N. Duda, D. J. Mooney, *Nat. Mater.* **2016**, *15*, 326.
[30] I. Mobasherpour, M. S. Heshajin, A. Kazemzadeh, M. Zakeri, *J. Alloys Compd.* **2007**, *430*, 330.
[31] M. W. Pfaffl, *Nucleic Acids Res.* **2001**, *29*, e45.